

Complete Nonlinear Magnetic-Thermal-Stress Design of Radial Field Multipole NdFeB Permanent Magnet Cylinder

Marius Rosu

Ansoft Corporation
225 West Station Square
Pittsburgh, PA 15219 USA

Scott Stanton

Ansoft Corporation
225 West Station Square
Pittsburgh, PA 15219 USA

John R. Brauer

Milwaukee School of Engineering
c/o P.O. Box 402
Fish Creek, WI 54212 USA

Zoltan J. Cendes

Ansoft Corporation
225 West Station Square
Pittsburgh, PA 15219 USA

Abstract - This paper presents a complete modeling approach for the analysis of the magnetization of a radial field multipole NdFeB permanent magnet cylinder. The simulation approach involves the 3D finite element parametric study of a permanent magnet rotor structure to extract electromagnetically equivalent state space variables. These variables are transferred to a circuit simulator where the genetic algorithm is used to optimize the circuit parameters of the magnetizing fixture. To validate the results of the optimized solution, a 3D time-stepping finite element analysis coupled with an embedded circuit simulator is employed. Further, a transient thermal analysis is performed to determine the effect of the resistive losses in the permanent magnet during the electromagnetic pulse. The high forces generated during magnetization process are solved by means of a 3D finite element analysis static stress simulation and the structural deformation is computed.

I. INTRODUCTION

The magnetization of permanent magnet cylinders has become a key element in the manufacture of permanent magnet electrical machines and can exert a considerable influence on final machine performance. However, the physics underlying this magnetization process is quite complicated and involves the rapid discharge of a capacitive power source, nonlinear permeabilities, eddy currents, thermal effects and mechanical stresses and deformations. Heuristic models of this magnetization process provide insufficient detail for design analysis and optimization.

Existing studies have focused on capacitor discharge magnetizers, modeling the differential equations governing the electric circuit and the nonlinear transient electromagnetic field equations [1] [2]. An air-cored impulse magnetizing fixture design methodology is presented in reference [3] where the authors used analytical methods and 2D time-stepping finite element analysis to show the influence of eddy currents on the design.

In this paper, a comprehensive 3D design procedure is presented for radial-field multipole impulse magnetizing fixtures. We show that a reasonably accurate equivalent circuit model of the permanent magnet can be generated by using parametric three-dimensional quasi-static finite element analysis. This equivalent circuit model can then be used in circuit simulation to model the capacitive discharge magnetization process. Since this circuit model runs very quickly, it is amenable to optimization via the genetic algorithm. The resulting optimized design can be validated and further refined by solving the design using complete time-stepping finite element analysis

and by coupling this transient electromagnetic simulation to thermal and structural simulation.

The techniques used in the design analysis are illustrated by a case study of a 6-pole brushless permanent magnet machine.

II. DESIGN ANALYSIS APPROACH AND RESULTS

The geometry of a six poles magnetizing fixture is presented in the Figure 1. In previous studies [4] [5], end effects were ignored and a simplified 2D model was employed. To avoid these errors, this paper uses a 3D model, although the stator is taken to be longer than the rotor in order to reduce end effects.

The different grades of isotropic NdFeB powder, produced by the rapid solidification process, currently dominate the high-performance polymer bonded magnet market [6]. Doubtless, they are challenged by the emerging anisotropic NdFeB powders, obtained from either the rapid solidification powder [7] or the Hydrogen - Decomposition - Desorption - Recombination (HDDR) [8].

In isotropic bonded magnets, the orientation of the magnetization is parallel to the direction of the magnetizing field regardless the orientation of the external applied field. Thus, any deviation of the magnetizing field from the desired orientation will result in a corresponding deviation of the remnant magnetic field. By contrast, for the anisotropic magnets, the orientation of the remnant magnetic field is established by the preferred axis of magnetization (easy axis) which is generated during the manufacturing process by the application of an aligning magnetic field prior to pressing or extreme mechanical deformation. Consequently, for anisotropic magnets the direction of the applied magnetizing field is not as critical in determining the orientation of the remanent magnetic field, due to the generated magnetocrystalline anisotropy. However, in order to obtain the intrinsic magnetic properties in both isotropic and anisotropic magnetic materials, the applied magnetizing field must fully saturate the permanent magnet material.

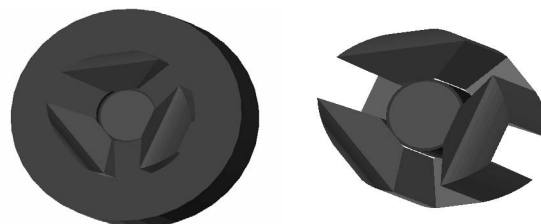


Figure 1. The stator-rotor electrical machine assembly

The axial length of a radial field magnetizing fixture should be as short as possible to minimize impedance and thus lower the stored energy in the capacitor and the pulse duration. However, making the magnetizing fixture the same length as the magnet which is to be magnetized is undesirable since the gap between the end-windings of the fixture and the magnet creates non-uniformity in the magnetization. In the case of isotropic magnet materials, the end-winding currents can result in a significant 2-pole axial component of magnetization. This not only reduces the achievable multipole radial-field but could result in unacceptable axial vibrations when the stator end-winding currents interact with the magnet assembled in an electric machine.

The nonlinear B(H) characteristic curves for the steel cores and permanent magnet material are shown in Figure 2. The stator core is laminated to reduce eddy-currents; the rotor core is solid. The permanent magnets were considered conductive with the conductivity set to 6.25E+05 S/m.

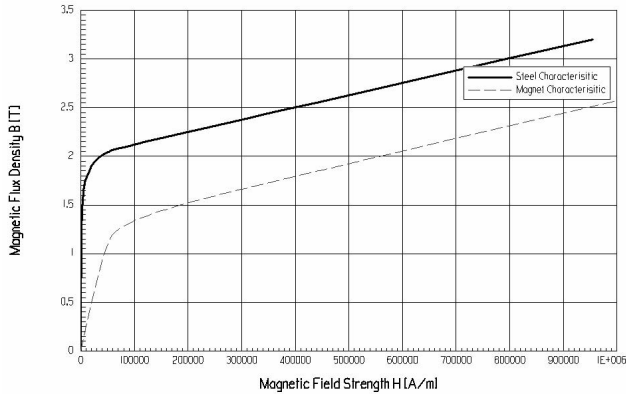


Figure 2. Magnetization curves for steel and magnet.

A. Parametric Analysis and System Design Optimization

A parametric 3D finite element analysis was first performed to get a complete range of coil inductance values. Inductance versus coil current is presented in Figure 3 under static conditions for the magnetization process assuming locked rotor conditions. The complete nonlinear lookup table based on the flux linkage computation was exported into the Simplorer™ circuit simulator as presented in Figure 4.

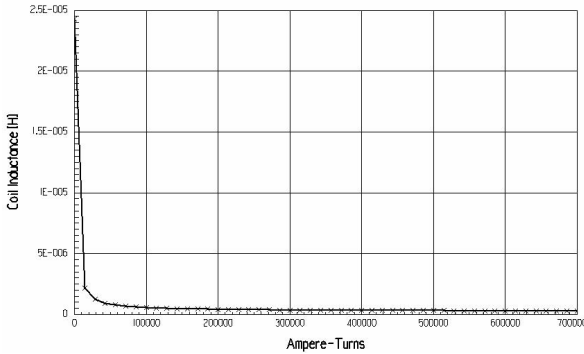


Figure 3. The coil inductance profile.

The main idea is to charge a capacitor to a certain initial voltage ($U_0 = 3\text{kV}$). Then the capacitor is discharged by turning on the switch at the time $t = 0$. This results in a current flow through the coil of the magnetizer. The discharge of this current through the coil of the magnetizer generates a magnetic field which penetrates the permanent magnet materials. When the voltage across the capacitor reaches 0 V at the time t , the current no longer flows through the circuit formed by C_1 , the winding, S_1 , AM_1 , L_{COIL} , R_{COIL} but instead flows through D_1 , R_{COIL} , L_{COIL} , and AM_1 . The components of the external inductor, $L_{winding}$ and $R_{winding}$ in Figure 4, limit the current in the main circuit and determine the time constant of the circuit. The inductor model in the external circuit ($L_{winding}$) takes the nonlinear magnetic characteristic into account as well as the geometric parameters of the magnetic core. The diode D_1 prevents an oscillating current from forming in the RLC circuit.

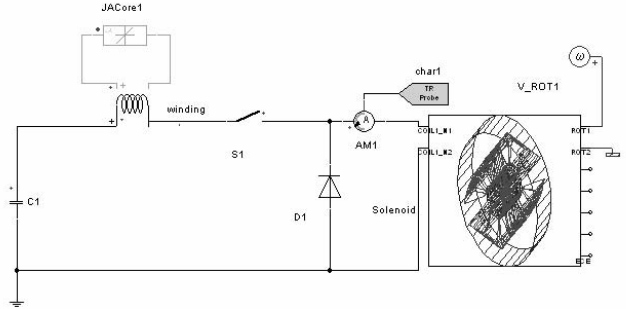


Figure 4. The entire system design concept of the magnetizing fixture.

The time domain circuit simulation includes the static electromagnetic behavior based on the finite element solution stored in a lookup table. This is appropriate at this stage of analysis since the response of the electromagnetic system is very fast. However, when the permanent magnet is exposed to a sudden change in the applied magnetic field, eddy currents are induced in the magnet. These currents shield the interior of the magnet from the magnetic field. The eddy currents decay with time and the magnetic field diffuses into the magnet. To estimate the time required for the magnetic field to penetrate the magnet, an infinitely long conducting and magnetically permeable homogeneous cylinder with radius a surrounded by air is analyzed. The field equations and boundary conditions governing this behavior are

$$\begin{cases} \nabla \times \vec{E} = -\frac{\partial \vec{B}}{\partial t} \\ \nabla \times \vec{H} = \vec{J} \\ \vec{J} = \sigma \vec{E} \\ \vec{B} = \mu \vec{H} \\ t < 0 \rightarrow H = H_1 \\ t = 0 \rightarrow H = H_2 \end{cases} \quad (1)$$

Assuming a special variation only in the radial direction r , the solution of this is

$$\left\{ \begin{array}{l} H(r,t) = H_2 \left(1 + 2 \left(\frac{H_1}{H_2} - 1 \right) \sum_{s=1}^{\infty} \frac{J_0(j_{0s}\xi)}{j_{0s} J_1(j_{0s})} \exp(-j_{0s}^2 \zeta) \right) \\ \xi = \frac{r}{a} \\ \zeta = \frac{t}{\sigma \mu a^2} \end{array} \right. \quad (2)$$

where, $\sigma \mu a^2$ is the diffusion time for the material with a magnetic permeability μ and an electric conductivity σ .

To optimize the external circuit parameters in respect to the peak value of the magnetizing current, the genetic algorithm was employed. The goal was to reduce the magnetization time by considering the diffusion of the magnetic field into the permanent magnet material and the value of the remanent magnetic field requirements at the end of the magnetization process.

The optimization analysis reported in [9] uses a genetic algorithm and a selected set of weighted performance measures. The simulation parameters are the genome of an initial population of individuals that is optimized by the genetic algorithm. The algorithm uses biological models including selection, recombination, and mutation over a series of transient simulation runs to produce an optimal population. The optimal population is produced over a specified number of generations from the initial population that has randomly distributed traits.

The optimization variables and their range of variation are shown in the Table 1. Optimization constraints are provided by the peak magnetizing current, the time of the peak magnetizing current t_m and the permanent magnet remnant flux density B_r . $I_{\text{peak}} < 7000$ A due to the force in the end-winding and the temperature rise in the permanent magnets, $t_m < 2.5$ ms due to the diffusion time and the temperature rise in permanent magnets and $B_r > 1.1$ T due to the remnant flux density in the permanent magnet.

The objective function was defined as a weighted expression of the above specifications. A multi-objective optimization was achieved by establishing different level of contributions of each individual characteristic (peak value of the magnetizing current, time of peak value of the magnetizing current and the remnant value of the permanent magnet when the magnetizing current goes to zero) to provide the total fitness of the system. The convergence of the computed objective function is displayed in Figure 5.

TABLE 1
THE OPTIMIZATION VARIABLES

VARIABLES	MINIMUM	MAXIMUM
Capacitance value	500 uF	10 mF
Inductor winding no. of turns	1	7
Saturation Magnetization	500E+03 A/m	1E+06 A/m
Effective area of core	500E-06 m ²	50E-03 m ²
Effective length of core	10 mm	50 mm

TABLE 2
THE OPTIMIZATION RESULTS

VARIABLES	OTIMUM VALUE
Capacitance value	2.4 mF
Inductor winding no. of turns	4
Saturation Magnetization	991210 A/m
Effective area of core	12.2E-03 m ²
Effective length of core	48.13 mm

The results of the optimization are presented in Table 2. We see the major role geometry and the magnetic characteristic of the external inductor play in the optimal design of the magnetizer. The optimized magnetization curve is shown in Figure 6. At the end of the magnetization process, a remnant magnetic flux density as high as 1.26T is achieved.

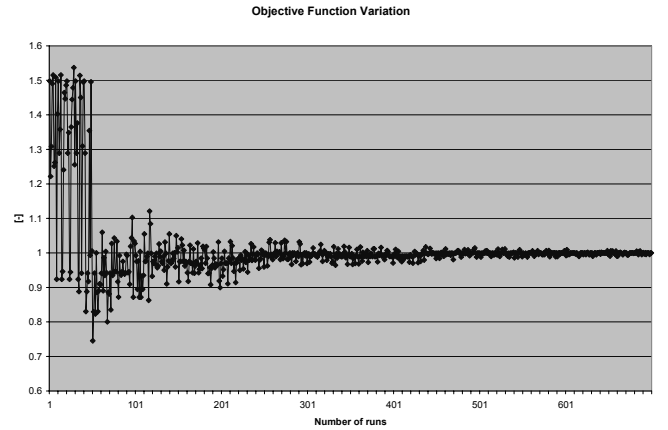


Figure 5. The objective function variation.

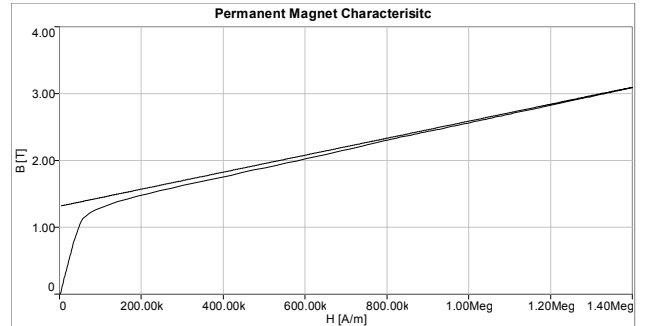


Figure 6. The B(H) profile of the permanent magnet.

B. Electromagnetic Transient Analysis of the Optimized System Design

To validate the results of the optimized solution, a coupled external circuit-3D time-stepping finite element analysis was performed. A new numerical technique of coupling finite elements with embedded circuits in the Maxwell simulator [10] was used to compute the fields and currents when the capacitor is discharged. Figure 7 illustrates the dynamic current response where the eddy-currents are fully computed in the finite element simulation.

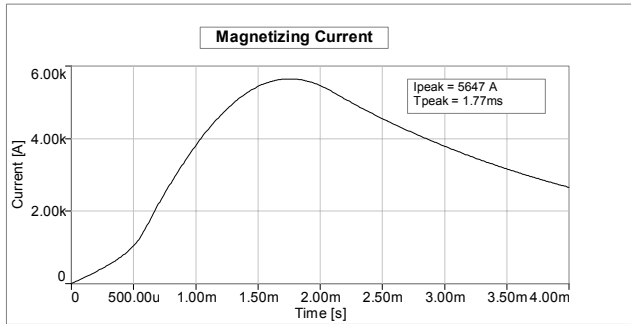


Figure 7. The winding current waveform during the magnetization process.

Figure 8 shows the capacitor voltage obtained from finite element transient analysis during the discharge period.

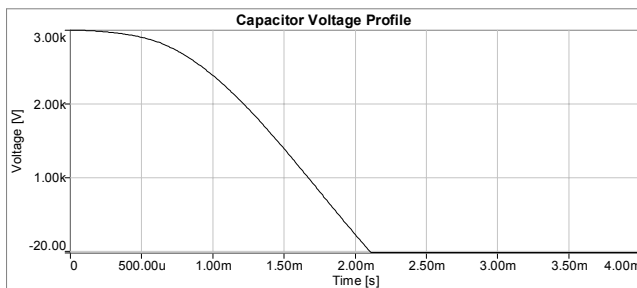


Figure 8. The capacitor voltage profile during the magnetization process.

The multipole structure and radial orientation of the magnetic field in the permanent magnets at peak current is shown in Figure 9.

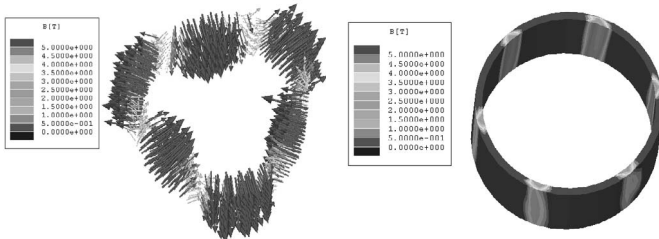


Figure 9. The radial multipole field generated during magnetization

C. Transient Thermal Analysis of the Optimized System

To accurately compute the temperature rise in the permanent magnet material due to the magnetizing pulse, the thermal time stepping technique reported in [11] was employed. During the electromagnetic time stepping analysis, the transient losses in the stator winding, the stator core, the permanent magnet material and the rotor core were estimated and used as input in the thermal simulation. Since the stator of the fixture was laminated, a core loss estimation procedure was employed to calculate the eddy, hysteresis and excess losses components as presented in Figure 10.

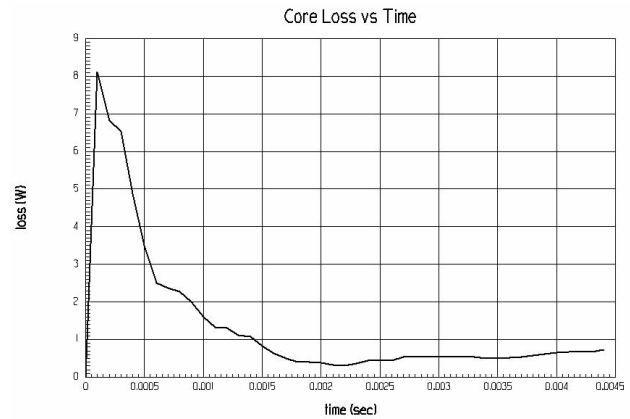


Figure 10. The transient core loss computation in the stator.

The stator winding structure has a stranded topology with 37 turns. Consequently, eddy currents in the winding are negligible; only ohmic losses are considered in Fig 11.

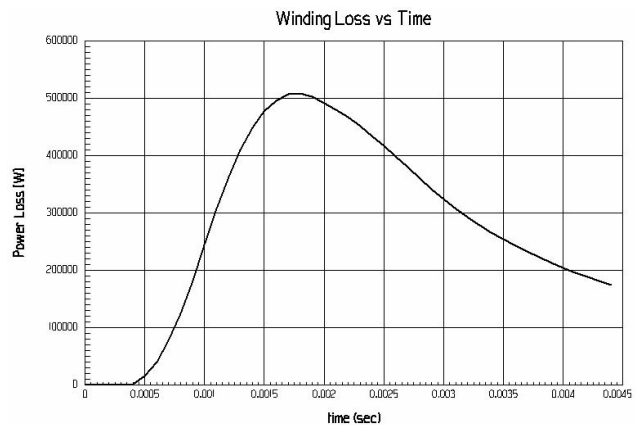


Figure 11. The transient winding loss computation.

Permanent magnets resistive losses due to the eddy currents developed during the magnetization process and their conductive property are shown in Figure 12.

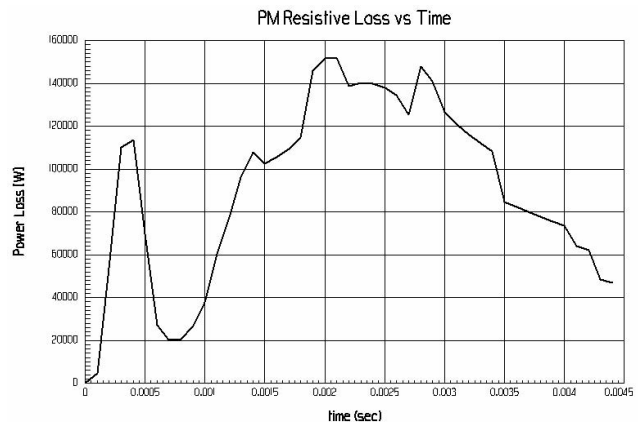


Figure 12. The transient permanent magnet resistive loss computation.

Figure 13 illustrates the rotor losses during the magnetization process. Since the rotor is solid, eddy-currents will pro-

vide the major contribution to total losses compared to hysteresis losses.

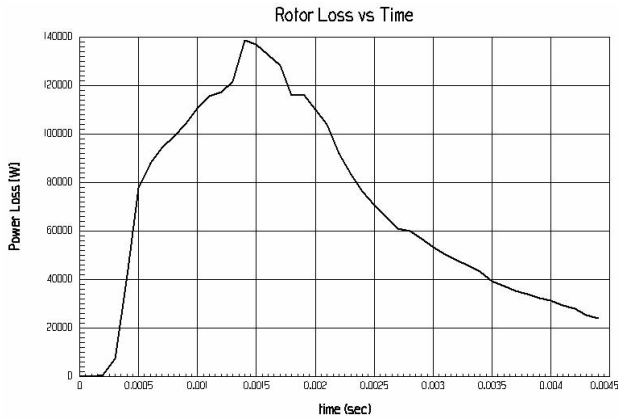


Figure 13. Transient rotor loss computation

The thermal performance of the magnetizer is strongly dependent on the temperature rise in the permanent magnet material and in the stator winding. Figures 14 and 15 illustrate the average temperature rise in the winding and permanent magnet material, respectively, during five consecutive pulses. Because of the short pulse duration, the thermal process in the winding is almost adiabatic, in agreement with expected physics. However, the energy dissipation in the permanent magnets results in a temperature rise of 6°C during the first pulse and almost 30.3°C by the end of five pulse cycles. This augmentation in temperature does not affect the saturation level of the permanent magnets.

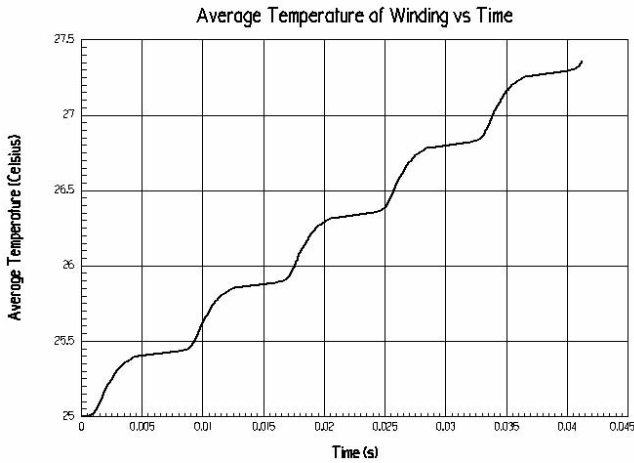


Figure 14. The winding temperature profile.

Figures 16 and 17 present the computed temperature variations along both an interior axial line and an exterior axial line in the permanent magnet. The thermal field computation clearly illustrates the accumulation of thermal energy in these materials over the duration of the magnetization process.

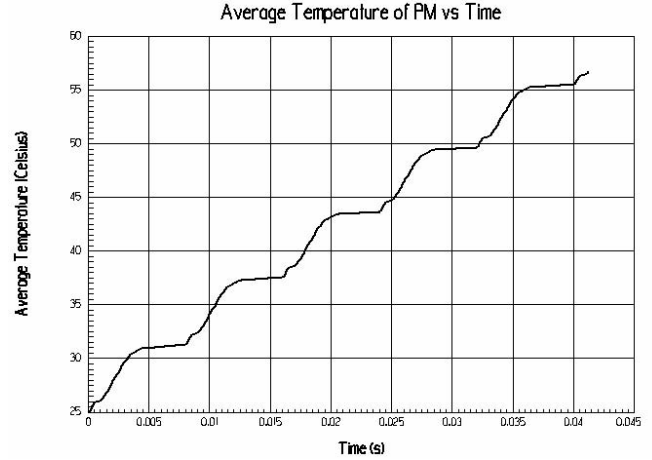


Figure 15. Permanent magnet temperature profile.

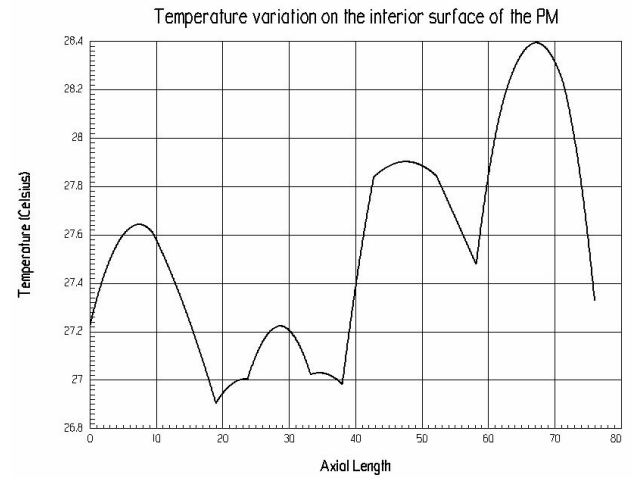


Figure 16. The computed temperature variation along an interior axial line on the surface of the permanent magnet material facing the rotor

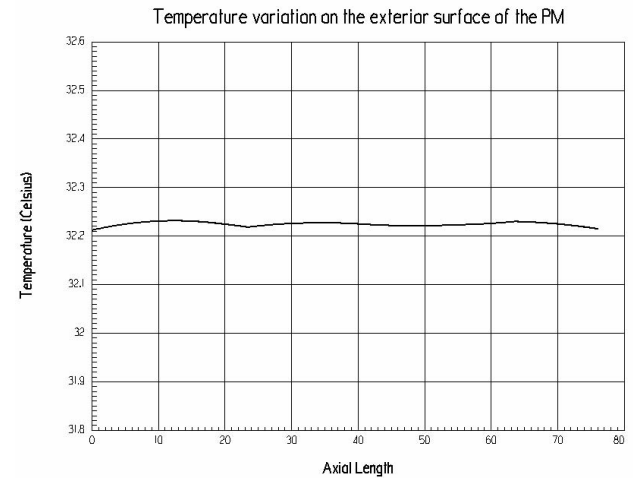


Figure 17. The computed temperature variation along an exterior axial line on the surface of the permanent magnet material facing the airgap

D. Static Stress Analysis of the Optimized System Design

A major factor that ultimately limits the achievable performance of a magnetizing fixture is the mechanical stress on the winding due to the high electromagnetic forces developed during the magnetizing process (see Figure 18). To properly model the structural deformation of the magnetizer, we employ a technology which couples 3D finite element electromagnetic time stepping analysis with 3D finite element static stress analysis [12]. Using this technology, transient forces are transferred to the static stress simulator as sources. Structural boundary conditions are defined according to the structural constraints of the magnetizer. The mesh topology of the electromagnetic transient simulation can be preserved for stress simulation or created anew using an adaptive algorithm.

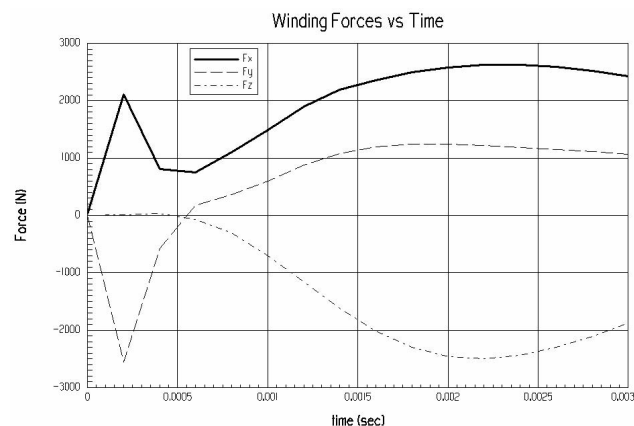


Figure 18. The winding transient electromagnetic force profile

Figure 19 shows the deformed shape of the end-winding due to peak transient force components acting on these parts.

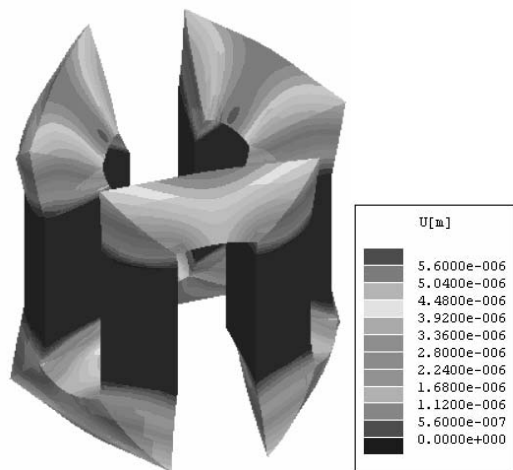


Figure 19. The end-winding static stress deformation profile

III. CONCLUSIONS

This paper presented a complete analysis of the operation of a magnetization fixture for magnetizing multi-pole ring NdFeB permanent magnets on the surface of a brushless cylindrical rotor. The analysis begins with a parametric 3D finite element analysis of the fixture and the cylinder to determine equivalent circuit parameters. Circuit simulation and the genetic algorithm are then employed to optimize the design parameters. The resulting design is further refined by combined transient 3D finite element-circuit simulation.

The local eddy-currents loss in each material is employed in 3D transient finite element thermal analysis to determine the temperature distribution in the permanent magnets.

The structural deformation due to the high magnetizing impulse current is evaluated by means of a coupled 3D finite element static stress simulator, taking into account the dynamic force signature computed during the magnetizing process.

REFERENCES

- [1] T. Nakata, and N. Takahashi, "Numerical Analysis of Transient Magnetic Field in a Capacitor-discharge Impulse Magnetizer," *IEEE Trans. Magnetics*, vol. 22, no. 5, pp. 526-528, 1986.
- [2] R. H. VanderHeiden, A. A. Arkadan and J. R. Brauer, "Nonlinear Transient Finite Element Modeling of a Capacitor-Discharge Magnetizing Fixture," *IEEE Trans. Magnetics*, vol. 29, no. 2, March 1993.
- [3] G. W. Jewell, D. Howe and C. D. Riley, "The Design of Radial-Field Multipole Impulse Magnetizing Fixtures for Isotropic NdFeB Magnets," *IEEE Trans. Magnetics*, vol. 33, no. 1, January 1997.
- [4] A. Binder, "Design of coils for magnetizing rotors with surface rare earth permanent magnets", *Proceedings of the International Conference on Electrical Machines, ICEM'96*, vol. III, pp. 449-454, Vigo, 1996.
- [5] T. Rylander, "Magnetization of Permanent Magnet Rotors - Theoretical and FEM Analysis -", *Master of Science Thesis*, Royal Institute of Technology, Stockholm, pp.124, 1997.
- [6] J. J. Croat, "Current status of rapidly solidified Nd-Fe-B permanent magnets," in *Proc. 13th Int. Workshop Rare-Earth Magnets Appl.*, Birmingham, Sept. 11-14, 1994.
- [7] M. Doser, R. W. Ribtich, J. J. Croat, and V. Panchanathan, "Bonded anisotropic NdFeB magnets from rapidly solidified powders," *J. Appl. Phys.*, vol. 69, no. 8, Apr. 1991.
- [8] N. Komada and M. Itoh, "Anisotropic Nd-Fe-B HDDR powder and its application for bonded magnets," in *Proc. Intertech Polymer Bonded Magnets 94 Conf.*, Chicago, Apr. 12-13, 1994.
- [9] *Simplorer Additional Modules*, User Manual, Ansoft Corporation, Pittsburgh, 2000.
- [10] P. Zhou, W. N. Fu, D. Lin, S. Stanton, and Z. J. Cendes, "Numerical modeling of magnetic devices," *IEEE Trans. Magnetics*, vol. 40, pp.1803-1809, July 2004.
- [11] Z. Badics, B. Ionescu, Z. J. Cendes, "High-Order Adaptive Time-Domain Solution of Nonlinear Coupled Electromagnetic-Thermal Problems," *IEEE Trans. Magnetics*, vol. 40, no.2, March 2004.
- [12] *Basics of the theory of deformable body mechanics (structural analysis)*, E-Physics Online Help, Ansoft Corporation Pittsburgh, 2004.